**International Journal of Power Electronics and Drive System (IJPEDS)**
Vol. 17, No. 1, March 2026, pp. 502~517
ISSN: 2088-8694, DOI: 10.11591/ijpeds.v17.i1.pp502-517 

# Investigation of efficiency and safety in wireless capacitive power transfer through a single-layer tissue phantom

**Yusmarnita Yusop[1], Amy Sarah Ngu[1], Cheok Yan Qi[1], N. B. Asan[1], Huzaimah Husin[1], Shakir Saat[2], Peter Adam Hoeher[3]**
[1]Centre of Telecommunication Research & Innovation, Faculty of Technology of Electronic and Computer Engineering, Universiti Teknikal Malaysia Melaka, Melaka, Malaysia
[2]Faculty of Engineering Technology and Science, Higher Colleges of Technology, Abu Dhabi, United Arab Emirates
[3]Kiel University, Kiel, Germany

**Article Info**

***Article history:***

Received Mar 29, 2025
Revised Jul 29, 2025
Accepted Dec 11, 2025

***Keywords:***

Capacitive power transfer
Class-E inverter
Electric field emission
LCCL impedance matching
Specific absorption rate

**ABSTRACT**

Wireless power transfer (WPT) is a promising solution for implantable biomedical devices, offering an alternative to traditional implanted batteries and percutaneous connections, which are limited by short lifespans and high infection risks. Existing capacitive power transfer (CPT) systems for biomedical implants often utilize media such as animal meat or liquids to validate power transfer across the human body, but these materials exhibit inconsistent and inaccurate dielectric properties. To address this limitation, this study proposes a CPT system designed to operate with a single-layer tissue phantom that closely mimics the dielectric characteristics of human tissue. The system is integrated with a class-E LCCL resonant topology to enhance power transfer efficiency. In addition to evaluating performance, this work also investigates safety aspects in terms of electric field emission and specific absorption rate (SAR). Simulations using MATLAB Simulink and ANSYS HFSS reveal that at a 1 mm tissue gap, the electric field reaches 298.09 V/m and the SAR is 1.14 W/kg, which are both within established safety limits (614 V/m and 2 W/kg per 10 g of tissue). Furthermore, a 5 W, 1 MHz system operating across a 2 mm tissue gap demonstrates power transfer efficiencies of 40.61% for skin tissue and 20.53% for muscle tissue. These results validate the system's safety and efficiency for powering deeply implanted biomedical devices.



***Corresponding Author:***

Yusmarnita Yusop
Centre of Telecommunication Research & Innovation (CeTRI)
Faculty of Technology of Electronic and Computer Engineering, Universiti Teknikal Malaysia Melaka
Melaka, Malaysia
Email: yusmarnita@utem.edu.my

## 1. INTRODUCTION

Wireless power transfer (WPT) is a technology that enables the transmission of electrical energy from a power source to an electrical load without using wires. It involves the transfer of power across a medium, allowing for the wireless transmission of energy. In the WPT system, the transmitter acts as the source of electrical power, receiving it from the power supply. It generates a time-varying electromagnetic field, which serves as the carrier for transmitting power across the medium. This electromagnetic field propagates wirelessly to the receiver, which captures the energy and supplies it to the intended load or device. Wireless power transfer technology is widely utilized across a diverse range of applications. These applications span from advanced low-power biomedical implants [1]-[3] to high-power electric vehicles [4],

[5] and everyday consumer products [6], [7] like electric toothbrushes and mobile phones. The versatility of WPT enables its use in various industries, providing convenient, safe, and efficient power delivery for a wide array of devices. A general WPT system has a transmitter unit and a receiver unit, which are separated by a medium that transfers energy between them, as illustrated in Figure 1. The transmitter and receiver units of the WPT system are not electrically connected, allowing for free movement in both linear and rotational modes. This provides flexibility, mobility, and safety for the loads being powered.

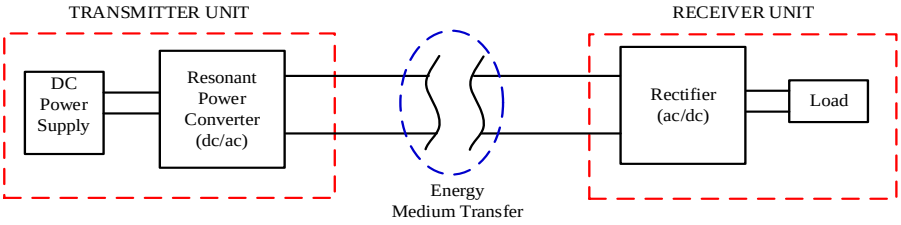


Figure 1. General block diagram of WPT system [8]

WPT has become a preferred technology in replacing conventional approach such as implanted batteries and percutaneous leads, that have several limitations as a long-term power supply for implantable biomedical devices (IBD), eliminating the use of wired power sources [9]. However, designing and implementing a high-efficiency WPT system in a biomedical implant is challenging. In the application of implanted biomedical devices, inductive power transfer (IPT) is the most common type of WPT due to its high-power level and ability to work with various gap distances. However, the presence of metallic shielding components makes it challenging to satisfy biocompatibility and hermeticity requirements in applying IPT, as the metal will shield the magnetic field from the receiver coil, leading to power losses [10], [11]. Moreover, miniaturization can lead to higher power densities, which can cause high field strengths and circulating currents [12]. These make it difficult to meet specific absorption rate (SAR) limits, which are concerned with human safety.

WPT technology can be classified into two categories, which are far-field and near-field. Near-field uses magnetic fields (inductive coupling) or electric fields (capacitive coupling) over short distances. Meanwhile, far-field uses electromagnetic radiation such as microwaves or lasers (acoustic radiation, optical radiation, microwave radiation) over longer distances. Among these technologies, near-field WPT is the most suitable in supporting implanted biomedical devices due to its ability in short transmission distance, which can guarantee the acceptable efficiency and power level [13], [14]. The proximity of energy medium transfer used in near-field results in high-power transfer efficiency (PTE).

For instance, the authors in [15]-[18] used an IPT system to supply power for IBD with a maximum transmit power ranging from 174 mW to 0.5 W, obtaining efficiency ranging from 36-63%. The authors in [19]-[21] used the CPT system to supply power for IBD with a maximum transmit power ranging from 150-287 mW, obtaining efficiency ranging from 54-70%. Moreover, a class-E amplifier has been used with an LCL impedance matching network for CPT in powering IBD, achieving up to 96.34% at 13.56 MHz with a maximum power of 5 W [1].

Hence, this paper focuses on the design of CPT in biomedical implants due to its ability to minimize power losses due to eddy current losses, cost-effectiveness, lightweight, and excellent performance even in cases of misalignment between transmitter and receiver plates. CPT systems can also transfer power through metallic shielding components using the electric field [22], addressing the challenge of IPT systems. The designed CPT system incorporates a class-E resonant inverter along with LCCL impedance matching networks to attain a power transfer efficiency of 100% theoretically by applying soft-switching conditions and compensating for the power losses caused by load and coupling variation. The class-E inverter, with a single switching element, efficiently handles high power and generates large currents at kilohertz to megahertz frequencies while minimizing switching losses. Besides that, integrating LCCL impedance matching with capacitive coupling plates can ensure uniform current flow into tissue, resulting in safer voltage stress.

The contribution of this paper can be explained as: i) Analysis of the CPT system for biomedical implants, integrating a class E resonant inverter with an LCCL impedance matching network. The system is experimentally validated using a single-layer tissue phantom configuration, providing a compact and realistic platform for investigating power transfer to biomedical implants; and ii) Comprehensive safety assessment of the proposed CPT system, including electric field emission and SAR evaluation through finite element method (FEM) simulations. The study considers different biological tissues, such as skin, fat, and muscle, within a single-layer phantom to ensure compliance with biomedical electromagnetic exposure standards.

## 2. SYSTEM OVERVIEW AND METHODOLOGY

### 2.1. Block diagram and system description

Figure 2 presents the overall architecture of the proposed CPT system for biomedical applications. The system consists of two main sections: the transmitter and the receiver, separated by a biological medium represented by a human tissue phantom. On the transmitter side, a DC power supply drives a class-E resonant inverter, which generates a high-frequency AC signal. This signal is then passed through an LC compensation network, which ensures impedance matching and maintains resonance, thereby improving power transfer efficiency. The energy is wirelessly transmitted across the tissue phantom via a four-plate capacitive coupling structure. In this structure, the transmitter forward plate and the return plate are positioned externally on the body surface, while the receiver forward plate and return plate are intended to be implanted inside the body. On the receiver side, a CL compensation network is used to further ensure resonance and proper impedance matching at the load interface. The received high-frequency AC signal is then converted back to DC using a full-bridge rectifier, which supplies power to an RL load representing the actual IBD load. The proposed CPT system is designed to evaluate both power transfer efficiency and biological safety, particularly by analyzing electric field distribution and SAR within the tissue during operation. These assessments are critical to ensuring that the system not only delivers sufficient power but also adheres to biomedical safety standards.

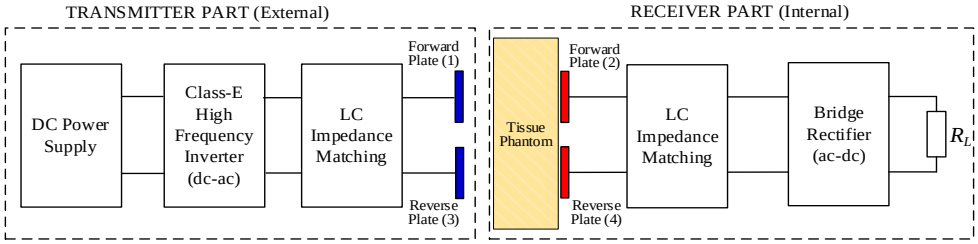


Figure 2. Proposed CPT system block diagram for IBD

### 2.2. Class-E LCCL topology design

The design specifications and circuit parameters of the class-E LCCL circuit are summarized in Table 1. Detailed calculations are not included here, as they have been thoroughly presented in our previous publication [23]. The component values are derived mathematically, following the methodology in [23], but recalculated based on new design specifications tailored for IBD applications. Figure 3(a) shows the schematic of class-E LCCL topology, which combines a class-E π1b circuit for transmitter compensation with an additional LC matching circuit for receiver compensation, forming a double-sided LC impedance matching circuit. This topology enhances efficiency by maintaining zero-voltage switching (ZVS), thereby reducing load sensitivity.

Table 1. Design specifications and circuit parameters of the class-E LCCL circuit

| Design specification | | | Circuit parameter | | Design value of |
|---|---|---|---|---|---|
| Parameter | Unit | Design value | Parameter | Unit | Class-E LCCL |
| $P_o$ | W | 5 | $L_f$ | µH | 500 |
| $f$ | MHz | 1 | $C_1$ | pF | 1759.048 |
| $V_{dc}$ | V | 12 | $L_1$ | µH | 26.439 |
| $D$ | | 0.5 | $C_2$ | pF | 948.284 |
| $Q_L$ | | 10 | $C_3$ | pF | 241.701 |
| $R_L$ | Ω | 50 | $C_4$ | pF | 843.45 |
| | | | $L_2$ | µH | 27.75 |

In the class-E LCCL circuit, the capacitor $C_3$ serves as the π1b matching component and coupling capacitance for the CPT system. Figure 3(b) shows Capacitor $C_3$ is modified into coupling plates, separating the class-E LCCL into transmitter and receiver parts. By referring to Table 1, $C_3$ = 241.701 pF. Therefore, by assuming that $C_{31} = C_{32}$, it can be calculated by using (1).

$$C_3 = \frac{C_{31} \times C_{32}}{C_{31} + C_{32}} = \frac{(C_{31})^2}{2C_{31}} = \frac{1}{2} C_{31} = \frac{1}{2} C_{32} \quad (1)$$

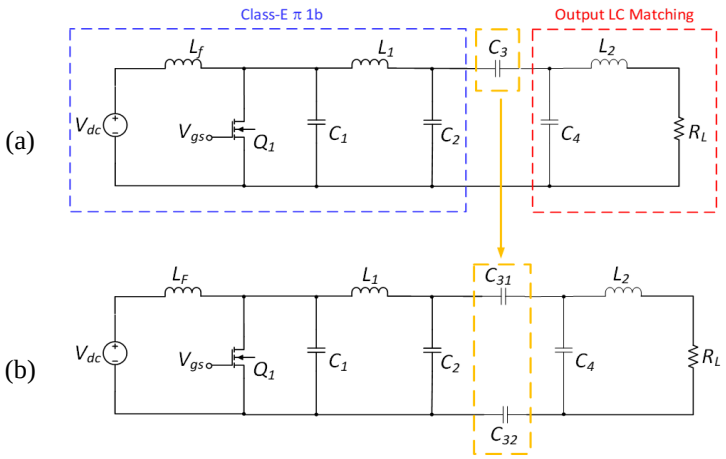


Figure 3. Class-E LCCL circuit: (a) class-E LCCL circuit with a single capacitor (b) transformation of a single capacitor into coupling plates

From (2) and (3), the capacitor $C_{31}$ and $C_{32}$ are twice the value of a single capacitor $C_3$ and will be replaced with circular copper plates. Capacitor $C_{31}$ corresponds to coupling plates 1 and 2, while the capacitor $C_{32}$ corresponds to coupling plates 3 and 4. The size of the coupling plates is determined using the area formula $A = \pi r^2$ where $A$ is the plate area, and $r$ is the plate radius. Thus, the capacitance can be analytically calculated as (2).

$$C = \frac{A.\varepsilon_o.\varepsilon_r}{d} \tag{2}$$

Therefore:

$$C_{31} = C_{32} = 2C_3 = \frac{2\varepsilon_0\varepsilon_r\pi r^2}{d} \tag{3}$$

where $\varepsilon_0$ is the permittivity of free space, $\varepsilon_r$ is the relative permittivity of the dielectric material, and $d$ is the separation distance between the plates. By rearranging the equation, the plate radius $r$ is expressed as (4).

$$r = \sqrt{\frac{2C_3 \times d}{2\varepsilon_0\varepsilon_r\pi}} \tag{4}$$

Based on the calculated plate radius from (4), the physical design of the coupling structure is determined while considering practical constraints such as alignment accuracy and fabrication tolerances. To prevent misalignment errors, the transmitter plate is larger than the receiver, but capacitance is calculated based on the overlapping area, aligning with theoretical analysis. From [24] the dielectric properties of human tissues at 1 MHz varied for each layer of skin, fat, and muscle. Hence, the average relative permittivity of the layered tissue can be analytically calculated as (5).

$$\varepsilon_{avg} = \sum_{i=1}^{N=1} r_i\varepsilon_i \ with\ r_i = \frac{d_i}{d_{total}} \tag{5}$$

### 2.3. Safety modeling using ANSYS FEM

The capacitance of the coupling plates must first be determined before performing the safety analysis in ANSYS Electronics Desktop. Both the forward and return plates are configured to have a capacitance of 478.63 pF. Based on (1) and the dielectric properties provided in Table 2, the designed four-plate coupler features a plate radius of 2.7 mm (corresponding to a 5.4 mm diameter) and a 1 mm initial tissue gap. The 1 mm separation is chosen to simulate a representative deep tissue scenario, where strong coupling is required under constrained spacing. Figure 4 illustrates the geometry setup used in the simulation environment, where the blue plate represents the transmitter, the red plate represents the receiver, and the yellow layer represents the human tissue phantom. Once the plate structure is simulated agreed well with the theory, then the analysis for electric field emission and SAR will be conducted based on the geometry setup.

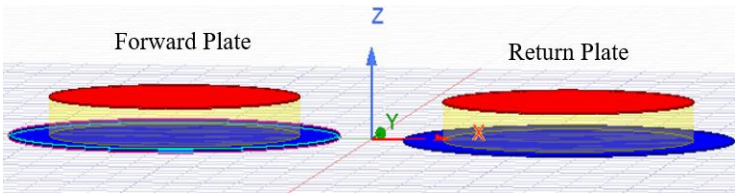


Figure 4. FEM geometry setup model

Table 2. Thickness and dielectric properties of tissues

| Tissue | Maximum thickness (mm) | $\varepsilon_r$ | $\sigma(s/m)$ | Tissue | Maximum thickness (mm) | $\varepsilon_r$ | $\sigma(s/m)$ |
|---|---|---|---|---|---|---|---|
| Dry skin | 3 | 990.76 | 0.0132 | Fat | 10 | 27.222 | 0.0251 |
| Wet skin | 3 | 1832.8 | 0.2214 | Muscle | 20 | 1836.4 | 0.5027 |

### 2.4. Experimental setup with tissue phantom

The tissue phantom utilized in this experiment was not developed specifically for this study; it was supplied by our research collaborator, who specializes in the fabrication of biomedical materials. Their work involves the design and validation of tissue phantoms that accurately replicate the dielectric characteristics of human tissue through precise formulation and rigorous testing procedures. All fabricated tissue phantoms must ensure that their dielectric properties align with the values specified in Table 2 to maintain biological accuracy and simulation reliability. Table 2 summarizes the thicknesses and dielectric properties of each tissue layer at 1 MHz, as defined by the Institute for Applied Physics [24]. For evaluation purposes, tissue phantoms with varying thicknesses will be fabricated. According to [25], the typical thicknesses of skin, fat, and muscle layers in the chest of an average adult male are 3 mm, 10 mm, and 20 mm, respectively.

The fabricated tissue phantom is then utilized in our research to examine the efficiency of capacitive coupling for wireless power transmission. The measurement setup, illustrated in Figure 5, measures the coupling capacitance across the tissue phantom layer. The capacitive coupling structure is configured in a sandwich arrangement, with a single-layer tissue phantom placed between two pairs of conductive plates. In this arrangement, the transmitter and return electrodes are placed externally, while the forward and return receiver plates are placed on the opposite side of the tissue layer, replicating a realistic transcutaneous energy transfer scenario for implanted biomedical devices. The capacitance of this structure is measured by using the KEYSIGHT E4990A impedance analyzer, which delivers a 1 MHz AC test signal to the coupling plates and calculates the resulting complex impedance. The effective capacitance is determined from this data. The system is set to achieve a target capacitance of 478.63 pF, consistent with the theoretical design values derived from (1). This experimental method accurately validates the capacitive coupling model, ensuring that the physical implementation matches the electrical characteristics needed for efficient power transfer and biomedical safety. Lastly, the class-E LCCL circuit is integrated with the verified capacitive coupling structure, allowing further experimental investigation of power transfer efficiency and performance across different tissue phantom thicknesses.

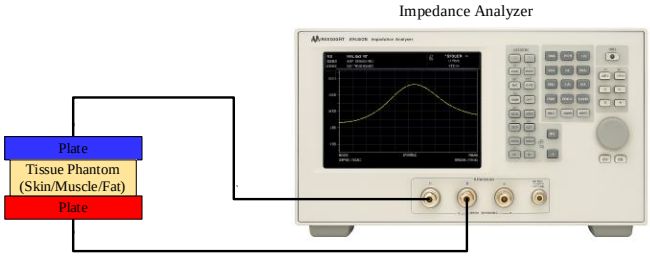


Figure 5. Impedance measurement setup for coupling capacitance with a single-layer tissue phantom

## 3. RESULTS AND DISCUSSION

### 3.1. Safety analysis

Initially, capacitance was simulated to ensure the plate's capacitance was accurate and within the expected range before proceeding with the electric field emission and SAR simulation. The simulated capacitance values are 478.48pF for the forward plate and 478.63 pF for the return plate, while the calculated

value using (1) is 483.4 pF. Table 3 shows error percentages of 1.02% and 0.99%, respectively, both under 5%, indicating high simulation accuracy in ANSYS Maxwell.

Table 3. Comparison of calculated and simulated capacitance values

| Parameter | Unit | Calculation | Simulation | Error percentage (%) |
|---|---|---|---|---|
| Capacitance of TX and RX forward plate, $C_{31}$ | pF | 483.4 | 478.48 | 1.02% |
| Capacitance of TX and RX return plate, $C_{32}$ | pF | 483.4 | 478.63 | 0.99% |

### 3.1.1. Electric field emission

Figure 6 illustrates the simulated electric field emission in ANSYS HFSS at varying human tissue gap distances. At 1mm, the highest E-Field reaches 298.09 V/m, with a uniform peak of 263.90 V/m in the central region tissue. At 5 mm, the maximum E-Field is 267.65 V/m, but the distribution is less uniform, with a central region dropping to 178.70 V/m. At 10 mm, the maximum E-Field is 267.70 V/m, with the lowest value at 50.64 V/m, showing a 72% and 81% reduction compared to 5 mm and 1 mm gaps, respectively. These results indicate that as the separation between electrodes increases, the electric field not only weakens in intensity but also becomes increasingly non-uniform across the tissue region. Despite these variations, all simulated electric field values remain well below the IEEE C95.1 human exposure limit of 614 V/m, ensuring that the system complies with established electromagnetic safety standards for biomedical applications.

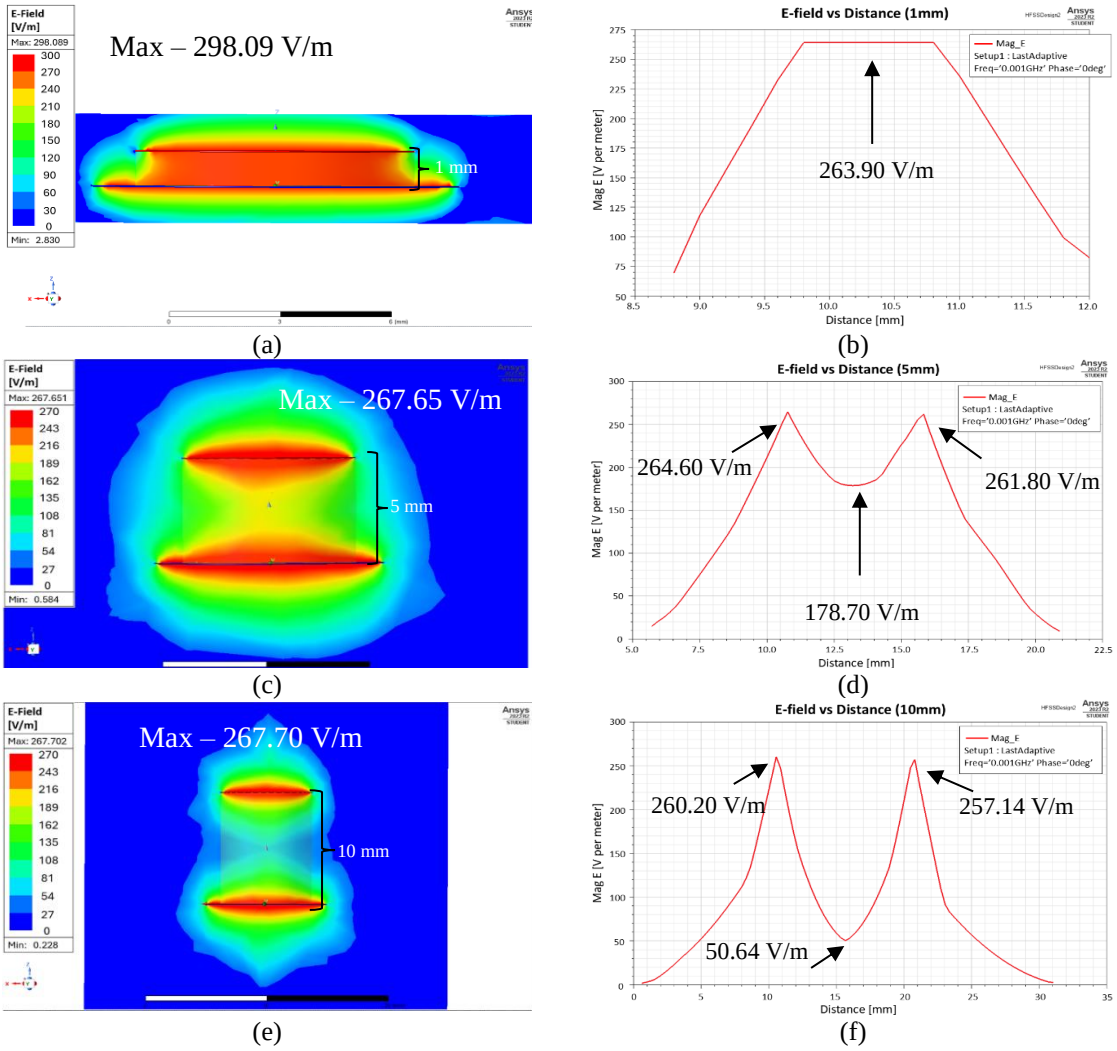


Figure 6. Electric field (e-field) emission analysis: (a) e-field distribution plot: 1 mm, (b) e-field vs distance: 1 mm, (c) e-field distribution plot: 5 mm, (d) e-field vs distance: 5 mm, (e) e-field distribution plot: 10 mm, and (f) e-field vs distance: 10 mm

### 3.1.2. Specific absorption rate

Figure 7 illustrates the simulated SAR distribution in human tissue at gap distances of 1 mm, 5 mm, and 10 mm using ANSYS HFSS. As the gap increases, the maximum SAR decreases, with values of 1.14 W/kg (1 mm), 0.77 W/kg (5 mm), and 0.62 W/kg (10 mm), aligning with theoretical expectations. In the central tissue, SAR values range from 0.86W/kg to 0.59 W/kg (1 mm), 0.71 W/kg to 0.08 W/kg (5 mm), and 0.56 W/kg to 0.02 W/kg (10 mm), showing significant reductions as distance increases. The peak SAR at 10 mm is notably lower than at 1 mm and 5 mm, confirming that SAR decreases with distance from the transmitter plate. All values remain well below the ICNIRP safety threshold of 2 W/kg for 10 g of tissue, ensuring compliance with safe exposure levels. In relation to the class-E LCCL topology, the resonant network reduces the voltage across the coupling capacitor ($C_3$), which lowers the electric field intensity, E = V/d. Since the SAR depends on the square of the electric field (SAR = $\sigma E^2/\rho$) where σ is the material conductivity and ρ is the density of the material, a lower field results in a significant reduction in SAR. This shows that the proposed circuit not only maintains efficiency through ZVS but also enhances safety by minimizing tissue exposure.

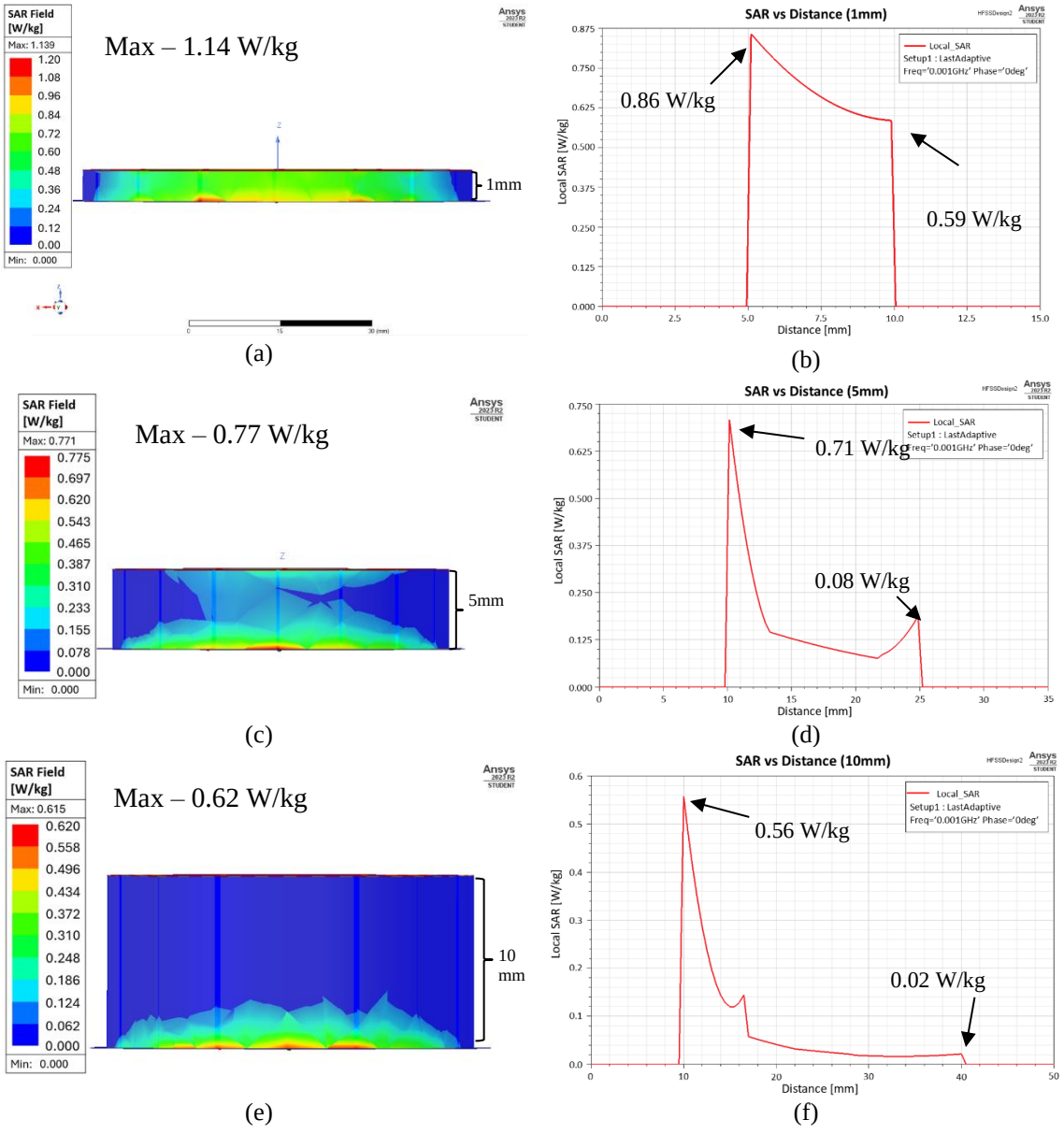


Figure 7. SAR analysis: (a) SAR distribution plot: 1 mm, (b) SAR vs distance: 1 mm, (c) SAR distribution plot: 5 mm, (d) SAR vs distance: 5 mm, (e) SAR distribution plot: 10 mm, and (f) SAR vs distance: 10 mm

### 3.2. Performance analysis of wireless CPT system based on class-E LCCL topology

#### 3.2.1. Class-E LCCL

The class-E LCCL system integrated with a full-wave rectifier was validated and evaluated in the laboratory, as shown in Figure 8. A TC4422 MOSFET gate driver, capable of delivering up to 9 A output current, was used to drive the IRF740 MOSFET in the transmitter circuit. The IRF740 was selected for its high-speed switching capability, 400 V breakdown voltage, and 10 A current rating, which meet the design requirements. Current and voltage measurements were obtained using a Keysight oscilloscope DSO-X 2012A and a Keysight current probe N2783B. The switching voltage waveforms are presented in Figure 9. A summary of the output performance from theoretical calculation, simulation, and experimental results is presented in Table 3. The $V_{GS}$ and $V_{DS}$ waveforms were analyzed for both simulation and experimental conditions. In the simulation, the maximum $V_{DS}$ during MOSFET turn-off, it reached 44.45 V, approximately three times $V_{dc}$ while during turn-on, it dropped to 0 V, consistent with theoretical expectations. Experimentally, the peak turn-off voltage $V_{DS(peak)}OFF$ was 50.7 V, 14.1% higher than the simulation, and the turn-on voltage was 1.6 V, about 3.2% of the peak turn-off voltage. These results confirm that the class-E LCCL circuit with a full-wave rectifier achieved the ZVS condition, with no overlap observed between $V_{GS}$ and $V_{DS}$ in either simulation or experiment.

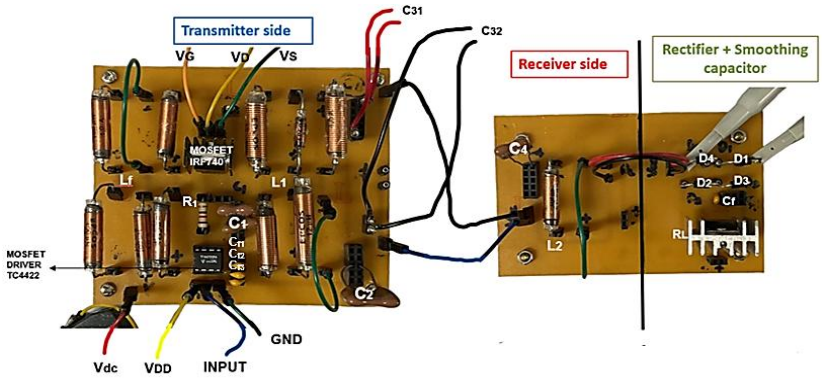


Figure 8. Circuit configuration of class-E LCCL with full-wave rectifier

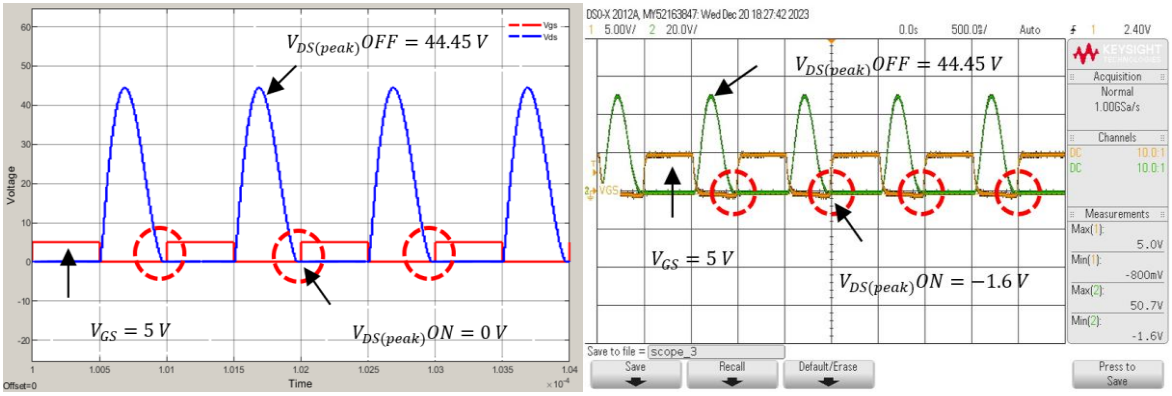


(a) (b)

Figure 9. ZVS waveform of class-E LCCL circuit: (a) simulation: MOSFET switching voltage and (b) experiment: MOSFET switching voltage

Table 3. Output performance of class-E LCCL circuit

| Parameter | Unit | Calculation | Simulation | Experiment |
|---|---|---|---|---|
| Input voltage, $V_{dc}$ | V | 12 | 12 | 11.96 |
| Input current, $I_{dc}$ | A | 0.42 | 0.42 | 0.4 |
| Input power, $P_{in}$ | W | 5 | 5 | 4.8 |
| Output voltage, $V_{RL(rms)}$ | V | 15.81 | 15.49 | 14.3 |
| Output current, $I_{RL(rms)}$ | A | 0.32 | 0.31 | 0.26 |
| Output power, $P_{out}$ | W | 5 | 4.8 | 3.7 |
| Efficiency, $\eta$ | % | 100 | 94.77 | 76.33 |

Figure 10 shows the input power measurement waveforms for the class-E LCCL circuit. Figure 11 shows the output power measurement waveforms for the class-E LCCL circuit. For the input and output power analysis, simulation results showed that an input current of 0.42 A at 12 V yielded 5 W input power, matching the calculated value. The output current of 0.31 A at 15.5 V produced 4.8 W output power, 4% lower than calculated, corresponding to an efficiency of 94.77%. Experimentally, the input current of 0.40 A at 11.96 V produced 4.8 W input power, 4% lower than the simulation. The output current of 0.26 A at 14.3 V resulted in 3.7 W output power, 22.9% lower than calculated, giving an efficiency of 76.33%. The experimental efficiency was 19.46% lower than the simulation results, primarily due to conduction, switching, and gate-drive losses, with additional contributions from the parasitic resistance of passive components further reducing the overall efficiency.

(a)

(b)

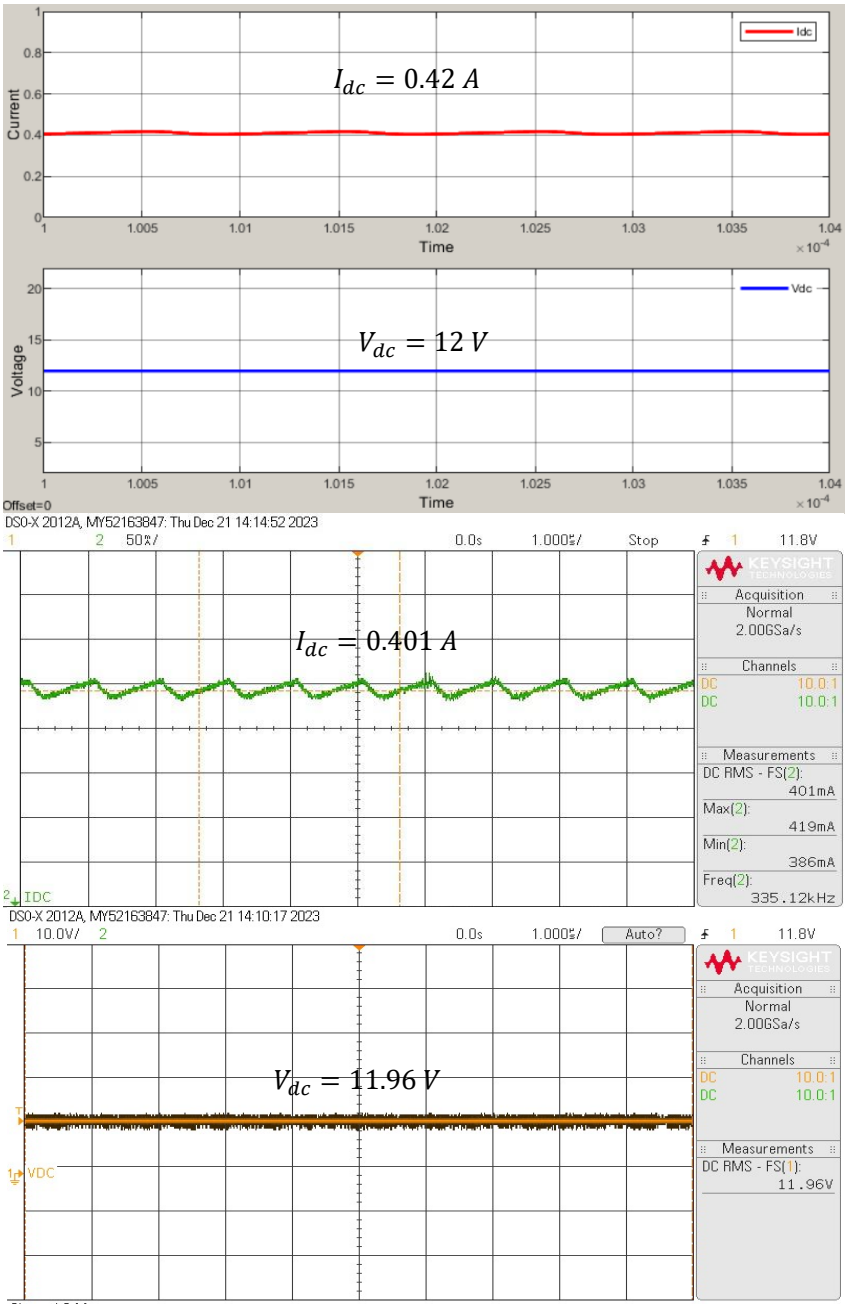


Figure 10. Input power measurement for the class-E LCCL circuit: (a) simulation: input current and voltage and (b) experiment: input current and voltage

Further validation was carried out by testing different gap distances between the capacitive plates at a fixed operating frequency of 1 MHz. This was achieved by adjusting the value of $C_3$ to represent the change in plate separation. At a 1 mm gap, the simulated efficiency was 94.77% with a calculated capacitance of 241.701 pF. The human tissue between the plates was modeled with a relative permittivity $\varepsilon_r$ of 1211.3. As the gap increased to 20 mm, the capacitance decreased exponentially, leading to higher reactance $X_{C3}$ reduced output current and voltage, and consequently lower efficiency, as shown in Figure 12(a). Overall, efficiency declined with increasing plate separation. Figure 12(b) presents the efficiency variation with different load resistances. The efficiency decreased from 95.9% to 74.4% as the load increased from 50 Ω to 658 Ω. This reduction is attributed to the impedance-matching nature of the class-E LCCL topology, which makes the efficiency less sensitive to load variations compared with non-matched systems.

(a)

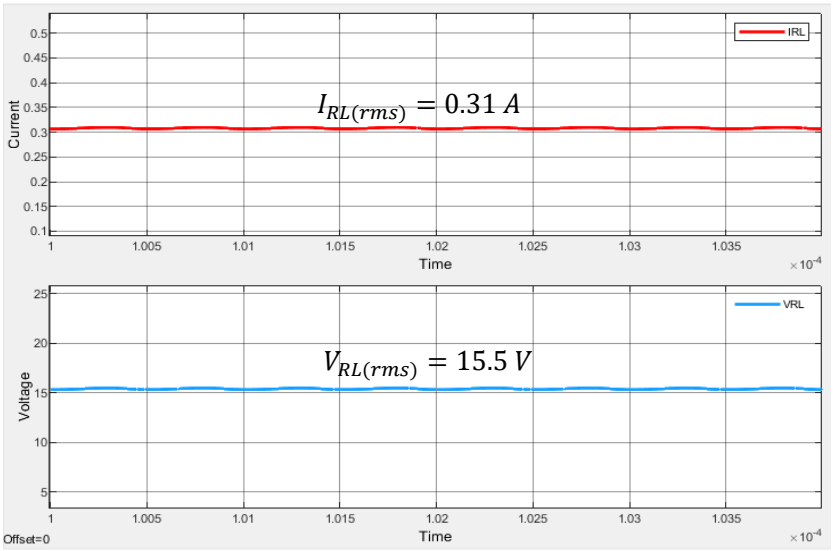


(b)

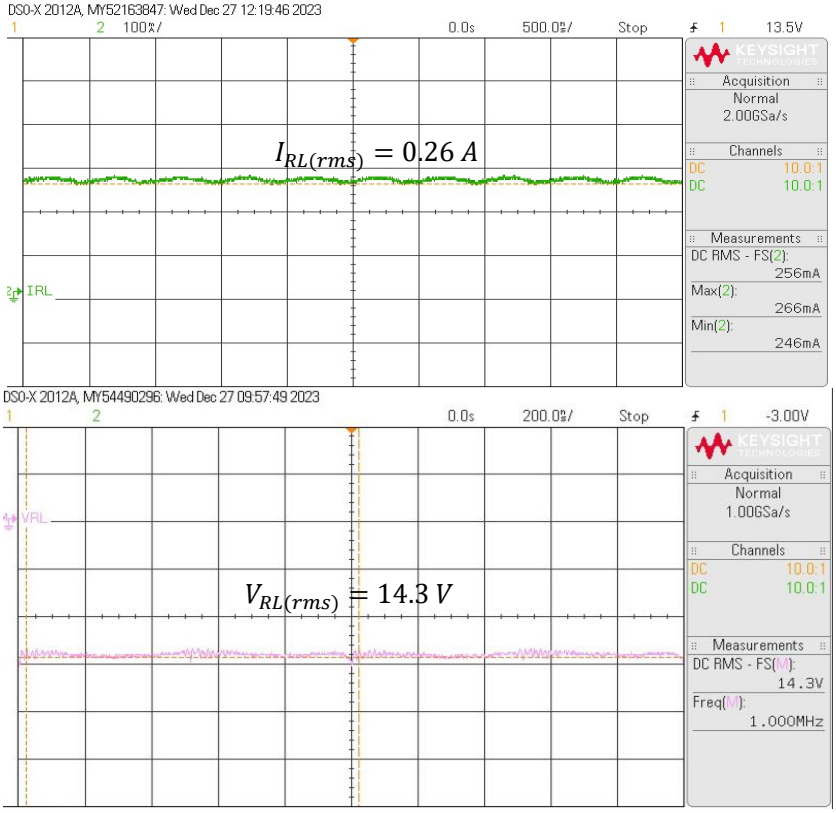


Figure 11. Output power measurement for the class-E LCCL circuit: (a) simulation: output current & voltage, and (b) experiment: output current and voltage

### 3.2.2. Wireless CPT system with single-layer tissue phantom

Figure 13 shows the experimental setup for the proposed wireless CPT system, featuring a class-E LCCL topology and capacitive coupling plates. Artificial agar-based human tissue is used as a phantom to mimic electrical properties and assess ZVS conditions, output power, and efficiency. Table 4 shows the output performances of the proposed system tested with a skin and muscle layer tissue phantom. Efficiency differences arise due to variations in input power ($P_{in}$) and output power ($P_{out}$). The skin tissue phantom achieves 40.61% efficiency, nearly 50% higher than the muscle tissue phantom (20.37%) at 1 MHz, likely due to differences in electrical properties. The initial class-E LCCL configuration yielded 76.33% efficiency, but testing with higher permittivity tissues and larger capacitive plates significantly reduced efficiency, impacting power transfer performance.

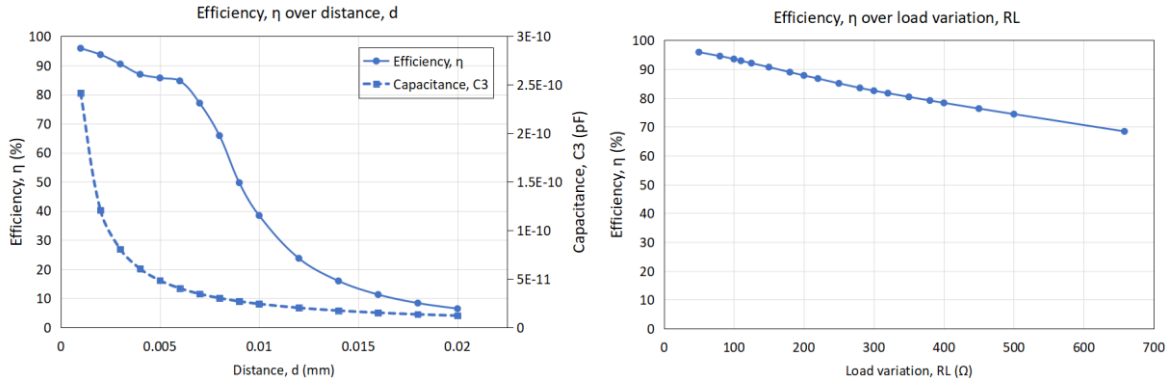


(a) (b)

Figure 12. Analysis of efficiency with gap distance and load variation: (a) plot of efficiency with varied gap distances and (b) plot of efficiency with varied load

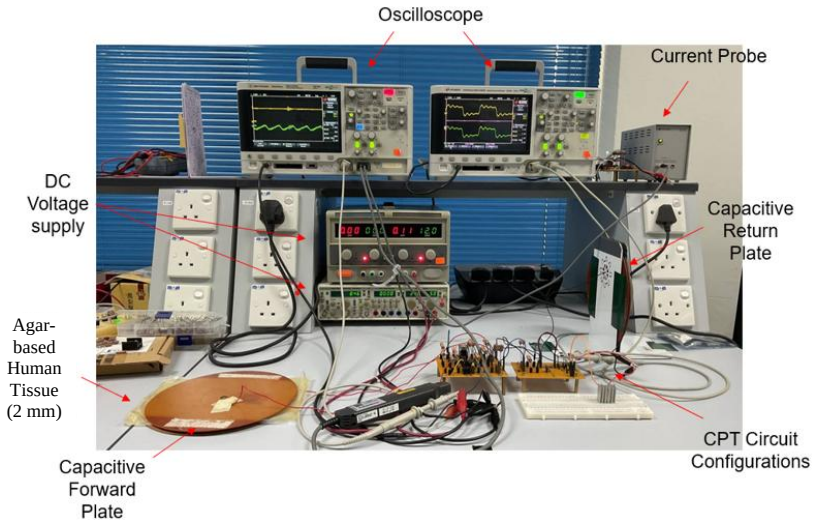


Figure 13. Experimental setup for the CPT system with a single-layer tissue phantom

Table 4. Output performances of the wireless CPT system tested with a skin and muscle tissue phantom

| Parameter | Unit | Experimental results (skin layer) | Experimental results (muscle layer) | Parameter | Unit | Experimental results (skin layer) | Experimental results (muscle layer) |
|---|---|---|---|---|---|---|---|
| $V_{dc}$ | V | 11.8 | 11.96 | $I_{RL(rms)}$ | mA | 12.3 | 4.7 |
| $I_{dc}$ | mA | 15.4 | 11.1 | $P_{out}$ | mW | 73.58 | 27.26 |
| $P_{in}$ | W | 0.18 | 0.13 | $\eta$ | % | 40.61 | 20.37 |
| $V_{RL(rms)}$ | V | 6.0 | 5.8 | | | | |

Figure 14 presents the switching voltage waveforms obtained from experiments using skin (as shown in Figure 14(a)) and muscle tissue phantoms (as shown in Figure 14(b)). In both cases, the switching voltage results confirm successful ZVS, as indicated by the absence of any overlap between $V_{GS}$ and $V_{DS}$. Figure 15 shows the input current and voltage waveforms obtained using skin and muscle tissue phantoms. For the power measurements, the skin tissue phantom test recorded an input current of 15.4 mA and an input voltage of 11.8 V, corresponding to an input power of 181.72 mW, which is notably lower than the theoretical 5 W.

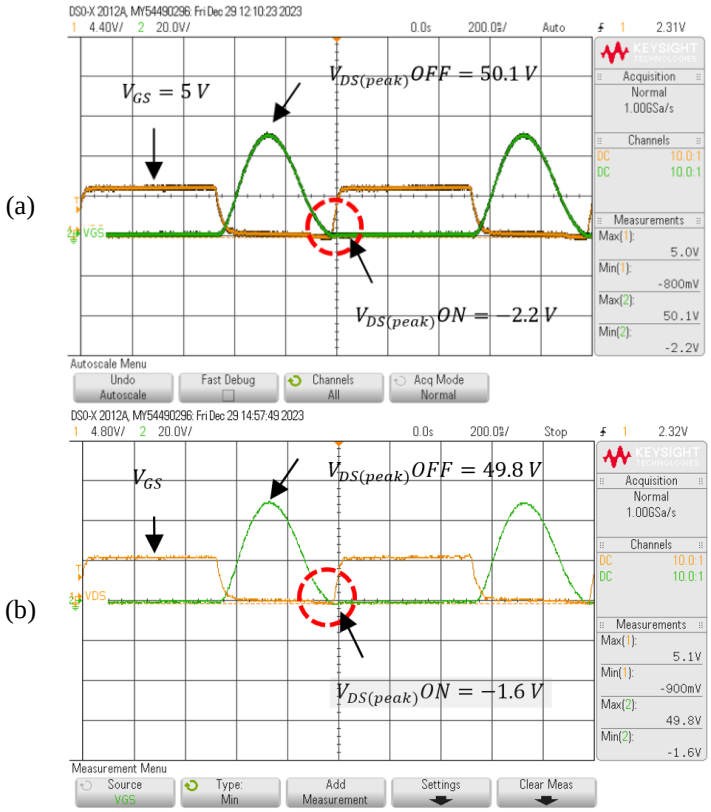


Figure 14. ZVS waveforms with tissue phantom: (a) skin: MOSFET switching voltages and (b) muscle: MOSFET switching voltages

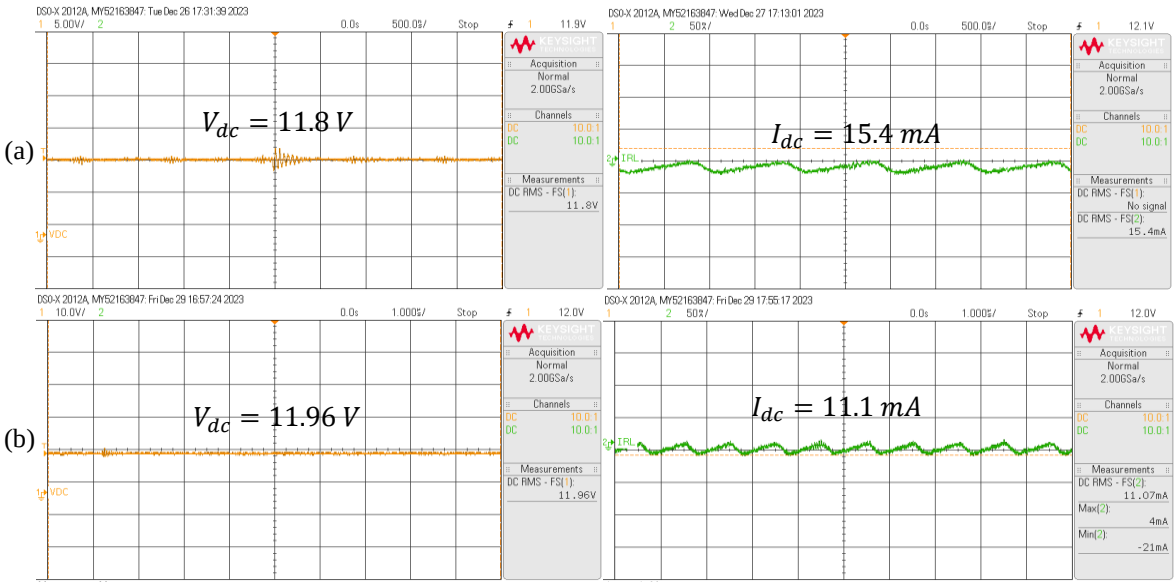


Figure 15. Input (current and voltage) with (a) skin and (b) muscle tissue phantom

Figure 16 depicts the output current and voltage waveforms obtained using skin and muscle tissue phantoms. The output current and voltage were 12.3 mA and 6.0 V, respectively, resulting in an output power of 73.8 mW and an efficiency of 40.61%. In the muscle tissue phantom test, the input current and voltage were 11.1 mA and 11.96 V, yielding an input power of 132.76 mW. The output current and voltage measured 4.7 mA and 5.8 V, producing an output power of 27.26 mW and an efficiency of 20.53%. The skin tissue phantom demonstrated higher efficiency compared to the muscle tissue phantom, likely due to its lower relative permittivity, which reduces dielectric losses at the operating frequency of 1 MHz, allowing a greater proportion of the transferred energy to reach the load.

Finally, the coupling gap distance between the plates with skin and muscle tissue phantoms was adjusted from 2 mm to 24 mm, representing the maximum human arm tissue thickness. This was achieved by adding layers to increase the phantom's thickness. As shown in Figures 17(a) and 17(b), the efficiency for both skin and muscle tissue phantoms steadily decrease with increasing gap distance. The decline occurs because a larger separation reduces the coupling capacitance exponentially, which raises the reactance $X_{C3}$ and consequently lowers the output current, output voltage, and overall efficiency.

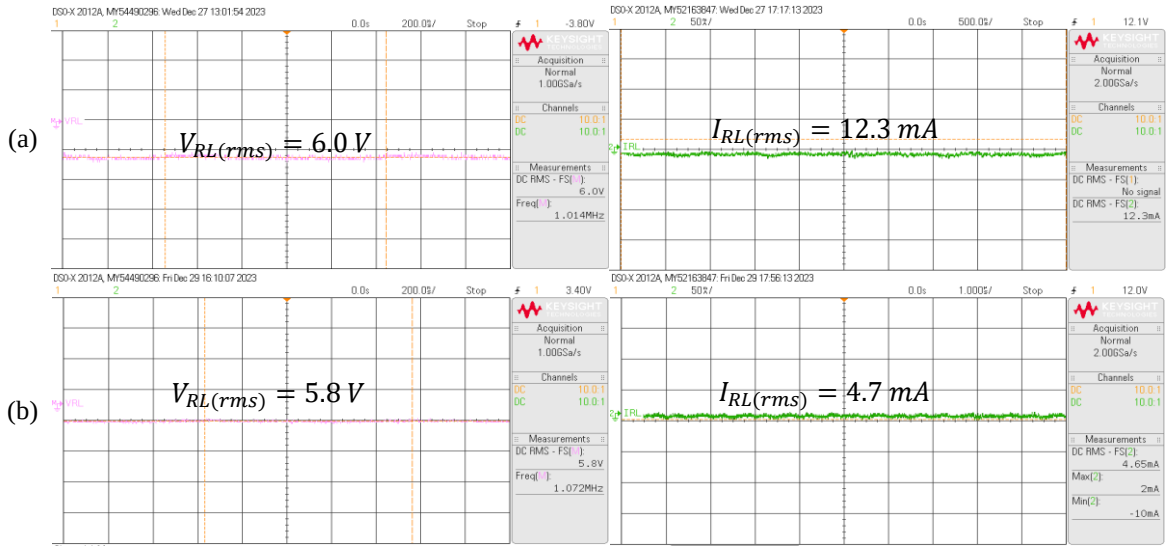


Figure 16. Output (current and voltage) power measurement with (a) skin and (b) muscle tissue phantom

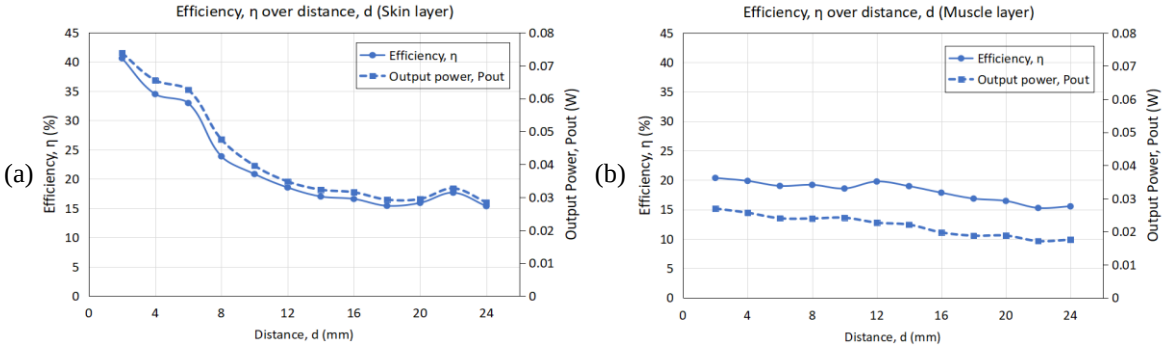


Figure 17. Analysis of efficiency with gap distance and load variation with (a) skin and (b) muscle tissue phantom

## 4. CONCLUSION

This study presented the design and evaluation of a wireless CPT system, emphasizing both safety and efficiency in biomedical applications. The proposed system, which integrates a class-E resonant inverter with an LCCL impedance matching network, was validated through simulation and experimental testing. Results demonstrated a high-power transfer efficiency of 94.77% in simulation and 76.33% in practice, delivering 3.7 W output power. Safety assessments confirmed that electric field emission and SAR remained within permissible

limits for separation distances ranging from 1 mm to 10 mm. When tested using a tissue phantom, the efficiency decreased to 40.61% for skin and 20.53% for muscle, primarily due to changes in coupling capacitance caused by the dielectric properties of the tissue materials. These findings highlight the trade-off between safety and efficiency, where increased separation improves safety but reduces efficiency due to lower coupling capacitance. Compared to existing CPT systems, the lower efficiency observed is attributed to differences in the effective capacitive coupling introduced by the tissue phantom. To further enhance the system's performance and robustness, several research directions are currently being pursued. First, the modelling of an equivalent multilayer tissue is planned to accurately predict power transfer characteristics and energy losses across the tissue phantom. Second, a frequency-dependent analysis of tissue phantom properties will be conducted to identify the optimal operating frequency for biomedical implants. Third, the system will be enhanced with AI-based adaptive tuning algorithms capable of dynamically adjusting parameters such as impedance matching and switching frequency in response to real-time variations in tissue properties or alignment, ensuring consistent and reliable power delivery. These future improvements aim to optimize the performance, adaptability, and clinical viability of capacitive wireless power transfer systems for next-generation implantable medical devices.

## ACKNOWLEDGMENTS

The authors acknowledge the financial support from the Ministry of Higher Education Malaysia and Universiti Teknikal Malaysia Melaka (UTeM), as well as the use of UTeM laboratory facilities and the assistance of laboratory engineers at the ASECS Laboratory.

## FUNDING INFORMATION

This work was supported in part by Universiti Teknikal Malaysia Melaka (UTeM) and Ministry of Higher Education Malaysia (MoHE) through the Fundamental Research Grant Scheme, FRGS/1/2023/TK07/ UTEM/02/3.

## AUTHOR CONTRIBUTIONS STATEMENT

This journal uses the Contributor Roles Taxonomy (CRediT) to recognize individual author contributions, reduce authorship disputes, and facilitate collaboration.

| Name of Author | C | M | So | Va | Fo | I | R | D | O | E | Vi | Su | P | Fu |
|---|---|---|---|---|---|---|---|---|---|---|---|---|---|---|
| Yusmarnita Yusop | ✓ | ✓ | | | | ✓ | ✓ | | | ✓ | ✓ | ✓ | ✓ | ✓ |
| Amy Sarah Ngu | ✓ | ✓ | ✓ | ✓ | ✓ | ✓ | | ✓ | ✓ | ✓ | ✓ | | | |
| Cheok Yan Qi | | ✓ | ✓ | ✓ | ✓ | ✓ | | ✓ | | ✓ | ✓ | | | |
| N. B. Asan | | ✓ | | | ✓ | | ✓ | | | ✓ | | | | |
| Huzaimah Husin | | ✓ | | | | ✓ | | | | ✓ | | | | ✓ |
| Shakir Saat | | ✓ | | | ✓ | | | | | ✓ | | ✓ | | |
| Peter Adam Hoeher | | ✓ | | | | ✓ | | | | ✓ | | ✓ | | |

C : **C**onceptualization
M : **M**ethodology
So : **So**ftware
Va : **Va**lidation
Fo : **Fo**rmal analysis
I : **I**nvestigation
R : **R**esources
D : **D**ata Curation
O : Writing - **O**riginal Draft
E : Writing - Review & **E**diting
Vi : **Vi**sualization
Su : **Su**pervision
P : **P**roject administration
Fu : **Fu**nding acquisition

## CONFLICT OF INTEREST STATEMENT

The authors declare no conflict of interest.

## DATA AVAILABILITY

The authors confirm that the data supporting the findings of this study are available within the article.

## REFERENCES

[1] N. R., V. A., B. Chokkalingam, S. Padmanaban, and Z. Leonowicz, "Class-E power amplifier design and optimization for the capacitive coupled wireless power transfer system in biomedical implants," *Energies*, vol. 10, no. 9, 2017, doi: 10.3390/en10091409.
[2] M. Z. Bin Mustapa, S. Saat, Y. Yusof, and M. M. Shaari, "Capacitive power transfer in biomedical implantable device: a review," *International Journal of Power Electronics and Drive Systems (IJPEDS)*, vol. 10, no. 2, p. 935, Jun. 2019, doi: 10.11591/ijpeds.v10.i2.pp935-942.
[3] M. Tamura, T. Segawa, and M. Matsumoto, "Capacitive coupler for wireless power transfer to intravascular implant devices," *IEEE Microwave and Wireless Components Letters*, vol. 32, no. 6, pp. 672–675, Jun. 2022, doi: 10.1109/LMWC.2022.3160688.

[4] H. Zhang, F. Lu, H. Hofmann, W. Liu, and C. Mi, "A 4-plate compact capacitive coupler design and lcl-compensated topology for capacitive power transfer in electric vehicle charging applications," *IEEE Transactions on Power Electronics*, pp. 1–1, 2016, doi: 10.1109/TPEL.2016.2520963.
[5] V.-B. Vu, M. Dahidah, V. Pickert, and V.-T. Phan, "An improved LCL-L compensation topology for capacitive power transfer in electric vehicle charging," *IEEE Access*, vol. 8, pp. 27757–27768, 2020, doi: 10.1109/ACCESS.2020.2971961.
[6] J. Lopez-Lopez, C. Salto, P. Zumel, C. Fernandez, A. Rodriguez-Lorente, and E. Olias, "High efficiency capacitive power transfer converter," in *2018 IEEE Applied Power Electronics Conference and Exposition (APEC)*, 2018, doi: 10.1109/APEC.2018.8341551.
[7] M. B. Lillholm, Y. Dou, X. Chen, and Z. Zhang, "Analysis and design of 10-MHz capacitive power transfer with multiple independent outputs for low-power portable devices," *IEEE Journal of Emerging and Selected Topics in Power Electronics*, vol. 10, no. 1, pp. 149–159, Feb. 2022, doi: 10.1109/JESTPE.2020.3035493.
[8] Y. Yusop, H. Husin, S. Saat, S. K. Nguang, and Z. Ghani, "Class-E LCCL for capacitive power transfer system," in *2016 IEEE International Conference on Power and Energy (PECon)*, Nov. 2016, pp. 428–433. doi: 10.1109/PECON.2016.7951600.
[9] Y. Zhou, C. Liu, and Y. Huang, "Wireless Power Transfer for Implanted Medical Application: A Review," *Energies*, vol. 13, no. 11, p. 2837, Jun. 2020, doi: 10.3390/en13112837.
[10] J. Bao, S. Hu, Z. Xie, G. Hu, Y. Lu, and L. Zheng, "Optimization of the coupling coefficient of the inductive link for wireless power transfer to biomedical implants," *International Journal of Antennas and Propagation*, vol. 2022, pp. 1–12, Jan. 2022, doi: 10.1155/2022/8619514.
[11] R. Sedehi, D. Budgett, A. P. Hu, and D. McCormick, "Effects of conductive tissue on capacitive wireless power transfer," in *2018 IEEE PELS Workshop on Emerging Technologies: Wireless Power Transfer (Wow)*, 2018, pp. 1–5. doi: 10.1109/WoW.2018.8450662.
[12] R. Sedehi *et al.*, "A wireless power method for deeply implanted biomedical devices via capacitively coupled conductive power transfer," *IEEE Transactions on Power Electronics*, vol. 36, no. 2, pp. 1870–1882, Feb. 2021, doi: 10.1109/TPEL.2020.3009048.
[13] H.-J. Kim, H. Hirayama, S. Kim, K. J. Han, R. Zhang, and J.-W. Choi, "Review of near-field wireless power and communication for biomedical applications," *IEEE Access*, vol. 5, pp. 21264–21285, 2017, doi: 10.1109/ACCESS.2017.2757267.
[14] D. Ahn and S. Hong, "Wireless power transmission with self-regulated output voltage for biomedical implant," *IEEE Transactions on Industrial Electronics*, vol. 61, no. 5, pp. 2225–2235, May 2014, doi: 10.1109/TIE.2013.2273472.
[15] S. Peng, M. Liu, Z. Tang, and C. Ma, "Optimal design of megahertz wireless power transfer systems for biomedical implants," in *2017 IEEE 26th International Symposium on Industrial Electronics (ISIE)*, Jun. 2017, pp. 805–810. doi: 10.1109/ISIE.2017.8001349.
[16] M. M. Omran, S. Mutashar, and A. Ezzulddin, "Design of an (8×8) mm 2 efficient inductive power link for medical applications," in *2019 2nd International Conference on Engineering Technology and its Applications (IICETA)*, Aug. 2019, pp. 61–66. doi: 10.1109/IICETA47481.2019.9012992.
[17] R.-F. Xue, K.-W. Cheng, and M. Je, "High-efficiency wireless power transfer for biomedical implants by optimal resonant load transformation," *IEEE Transactions on Circuits and Systems I: Regular Papers*, vol. 60, no. 4, 2013, doi: 10.1109/TCSI.2012.2209297.
[18] S. Nag, A. Koruprolu, S. M. Saikh, R. Erfani, and P. Mohseni, "Auto-resonant tuning for capacitive power and data telemetry using flexible patches," *IEEE Transactions on Circuits and Systems II: Express Briefs*, vol. 67, no. 10, 2020, doi: 10.1109/TCSII.2019.2955568.
[19] R. Erfani, F. Marefat, A. M. Sodagar, and P. Mohseni, "Modeling and experimental validation of a capacitive link for wireless power transfer to biomedical implants," *IEEE Transactions on Circuits and Systems II: Express Briefs*, vol. 65, no. 7, pp. 923–927, Jul. 2018, doi: 10.1109/TCSII.2017.2737140.
[20] R. Erfani, F. Marefat, and P. Mohseni, "Biosafety considerations of a capacitive link for wireless power transfer to biomedical implants," in *2018 IEEE Biomedical Circuits and Systems Conference (BioCAS)*, 2018, pp. 1–4. doi: 10.1109/BIOCAS.2018.8584827.
[21] L. Huang, A. P. U, A. Swain, S. Kim, and Yijun Ren, "An overview of capacitively coupled power transfer — A new contactless power transfer solution," in *2013 IEEE 8th Conference on Industrial Electronics and Applications (ICIEA)*, Jun. 2013, pp. 461–465. doi: 10.1109/ICIEA.2013.6566413.
[22] X.-D. Qing, Z.-H. Wang, Y.-G. Su, Y.-M. Zhao, and X.-Y. Wu, "Parameter design method with constant output voltage characteristic for bilateral LC-compensated CPT system," *IEEE Journal of Emerging and Selected Topics in Power Electronics*, vol. 8, no. 3, pp. 2707–2715, Sep. 2020, doi: 10.1109/JESTPE.2019.2936231.
[23] Y. Yusop, C. Y. Qi, S. Saat, H. Husin, and R. Shaktivel, "Simulation analysis of double-sided LC network for wireless capacitive transcutaneous energy transfer," in *2023 International Conference on Engineering and Emerging Technologies (ICEET)*, Oct. 2023, pp. 1–6. doi: 10.1109/ICEET60227.2023.10525910.
[24] N. Carrara, "Dielectric properties of body tissues." http://niremf.ifac.cnr.it/tissprop/ (accessed Jun. 22, 2023).
[25] M. M. Rahman and G. M. Rather, "A simple and accurate FDTD-based technique to determine equivalent complex permittivity of the multi-layered human tissue in MICS band," *Journal of Science: Advanced Materials and Devices*, vol. 5, no. 1, pp. 134–141, Mar. 2020, doi: 10.1016/j.jsamd.2020.02.004.

## BIOGRAPHIES OF AUTHORS

**Yusmarnita Yusop** was born in Melaka, Malaysia, in 1979. She received a B.Eng. in electrical engineering (Mechatronic) from Universiti Teknologi Malaysia, in 2001, an M.Eng. degree in electrical engineering from Kolej Universiti Tun Hussein Onn, Malaysia, in 2004, and a Ph.D. degree in electrical engineering (Capacitive power transfer) from Universiti Teknikal Malaysia Melaka in 2018. Her career as an academician began in 2005 as a teaching engineer at the Department of Industrial Electronics, Technical University Malaysia Malacca, and now she is a senior lecturer at the same university. Her area of research interests includes electronic system design, wireless power transfer, and power electronics. She can be contacted at email: yusmarnita@utem.edu.my.

**Amy Sarah Ngu** was born in Sarikei, Sarawak in 2000. She obtained her bachelor's degree in Electronic Engineering from Universiti Teknikal Malaysia Melaka (UTeM), Melaka, Malaysia in 2024. She is currently working at Intel Corporation in Penang as a Package Design Engineer Graduate Trainee. Her area of research interests includes wireless power transfer, capacitive power transfer, Class-E power amplifier, and biomedical implantable devices. She can be contacted at email: amysarahngu24@gmail.com.

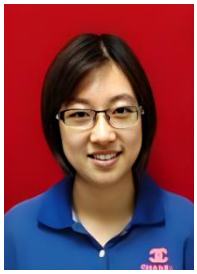

**Cheok Yan Qi** was born in Muar, Malaysia in 1995. She received the B.Eng. master's degree from Universiti Malaysia Melaka, Melaka, Malaysia in 2019 and 2023. She is now pursuing her Ph.D. degree in electronic engineering at Universiti Malaysia Melaka since September 2023. Her research field includes wireless power transfer systems specifically in capacitive power transfer. She can be contacted at email: p122310004@student.utem.edu.my.

**N. B. Asan** is a Senior Lecturer at the Department of Electronics Engineering, FTKEK, Universiti Teknikal Malaysia Melaka (UTeM), Malaysia. She received her Bachelor of Engineering in Electronic Engineering (Telecommunication Electronics) from UTeM in 2008 and her Master of Engineering in Communication and Computer from Universiti Kebangsaan Malaysia in 2012. She was awarded a Ph.D. in Engineering Science with a specialization in Microwave Technology from Uppsala University, Sweden, in 2019. Her research interests lie in the field of microwave engineering and biomedical applications, with a particular emphasis on compact antenna design for on-body and implantable systems, electromagnetic-based computer-aided antenna design, microwave sensors, intrabody wireless sensor networks, microwave material characterization, and human/animals tissue-equivalent phantom development. She is also actively involved in the design, optimization, and characterization of biomedical sensors for fat-intrabody microwave communication (fat-IBC). She can be contacted at email: noorbadariah@utem.edu.my.

**Huzaimah Husin** received her B.Eng. degree in 2000 from Multimedia University, followed by an M.Eng. degree in 2005 from Kolej Universiti Tun Hussein Onn, Malaysia. She began her academic career as an Engineering Instructor in 2001 at Kolej Universiti Teknikal Malaysia Melaka. She was subsequently appointed as a Lecturer in 2005 and later promoted to Senior Lecturer in 2008 in the Department of Industrial Electronics, Faculty of Electronic and Computer Engineering, Universiti Teknikal Malaysia Melaka. She received her Ph.D. in Advanced Control Technology in 2024, which focused on the Acoustic Power Transmitter Inverter Design. She can be contacted at email: huzaimah@utem.edu.my.

**Shakir Saat** was born in Kedah, Malaysia, in 1981. He received a B.Eng. and M.Eng. degrees in electrical engineering from the Universiti Teknologi Malaysia, Malaysia, in 2002 and 2006, respectively, and the Ph.D. degree in electrical engineering (Nonlinear control theory) from the University of Auckland, New Zealand, in 2013. He is now an associate professor of the Faculty Engineering and Science, at Higher Colleges of Technology, Abu Dhabi, United Arab Emirates. His research interest is in nonlinear systems control theory and wireless power transfer technologies. He has published one monograph (published by Springer Verlag) on polynomial control systems and many journals and conference papers mostly published in high-quality journals such as the International Journal of Robust and Nonlinear Control, and IET Control. He can be contacted at email: mmdsaat@hct.ac.ae.

**Peter Adam Hoeher** received the Dipl.-Ing. Degree in electrical engineering from RWTH Aachen University, Aachen, Germany, in 1986, and the Dr.-Ing. degree in electrical engineering from the University of Kaiserslautern, Kaiserslautern, Germany, in 1990. From 1986 to 1998, he was with the German Aerospace Center (DLR), Oberpfaffenhofen, Germany. From 1991 to 1992, he was on leave as a PostDoc at AT&T Bell Laboratories, Murray Hill, NJ. In 1998, he joined the University of Kiel, Germany, where he is a Full Professor of electrical and information engineering. His research interests are in the general area of digital communications, including simultaneous information and power transfer. Since 2014, he has been an IEEE Fellow. He can be contacted at email: ph@tf.uni-kiel.de.